water

MDPI

Article

A Thermal Model for Predicting the Performance of a Solar Still with Fresnel Lens

Ana Johnson [1], Lei Mu [1], Young Ho Park [1], Delia J. Valles [2], Huiyao Wang [3], Pei Xu [3], Krishna Kota [1] and Sarada Kuravi [1,*]

1 Department of Mechanical and Aerospace Engineering, New Mexico State University, Las Cruces, NM 88003, USA
2 Department of Industrial Engineering, New Mexico State University, Las Cruces, NM 88003, USA
3 Department of Civil Engineering, New Mexico State University, Las Cruces, NM 88003, USA
* Correspondence: skuravi@nmsu.edu; Tel.: +1-574-646-1587

Received: 2 August 2019; Accepted: 4 September 2019; Published: 7 September 2019

check for updates

Abstract: This study presents a theoretical model to simulate the temperatures and productivity of a single-slope, single-basin solar still when an external solar enhancement is used. Experiments were performed in the New Mexico region (32.3199° N, 106.7637° W) to validate the numerical model. A point focusing Fresnel lens was used in the experiments to enhance the solar input. It was found that a significant rise in the productivity of the still was achieved with the Fresnel lens. Parametric study by varying the water depth showed the Fresnel lens was more effective for larger water depths. In addition, the Fresnel lens can aid in improving the overall efficiency of the solar still.

Keywords: solar still; insolation; distillation; single-slope still; Fresnel lens; solar enhancement; desalination; productivity enhancement

1. Introduction

Meeting the increasing demand for fresh water is a grand challenge. Desalination and water reuse have become two key solutions to addressing water shortage and sustainability. Utilizing solar-powered treatment processes is especially appealing for the most arid and high irradiance regions in the world. Moreover, the use of this technology is an excellent choice for providing treated and desalinated water for small water systems, and communities in remote arid areas. These areas usually have access to saline and groundwater but limited/or no connections to electrical grids. The advantages of the use of solar energy also include the low maintenance, noise-free operation, long life, free sunlight, and non-emission of greenhouse gases.

Currently, desalination using solar energy is achieved by using solar thermal collectors, solar ponds, or solar photovoltaics [1,2]. Some processes convert solar energy into electrical energy whereas others utilize it to produce thermal energy. Optimization of membrane separation processes may utilize solar energy in multiple forms, such as generating electrical energy via photovoltaic (PV) panels combined with solar thermal preheating of feed water

The simple technology for direct desalination is by utilizing a solar still, where the heat collection and the distillation are achieved in the same equipment [3]. The basic concept of a solar still is simple. It consists of a basin filled with the saline/brackish water, blackened bottom surface for absorbing the radiation, and a transparent glass cover placed on top of it. When the solar radiation is incident on the glass cover, it passes through the glass and gets absorbed by the water and the absorber surface. Due to this, the water temperature and the vapor pressure increase and as a result, the vapor rises to the cover by natural convection and is condensed on the inner side of the cover. The condensate is collected at a collection trough which can be present at the end of the glass cover or can be separate.

Solar stills could be the most affordable choice in remote and arid areas. They produce fresh water directly without requiring any fuel or electricity to operate. However, the associated disadvantages are the low temperature of the water, low output of water production, and low performance efficiencies.

Solar stills can be classified into active and passive solar stills. Many papers have studied more specific characteristics of solar stills with various configurations, hemispherical solar stills [4], spherical solar still [5], pyramidal solar still [6], double-basin solar still [7–11], vacuum solar still [12], compound parabolic concentrator (CPC) solar still [5], wick type solar still [13], triple basin solar still [14], multiple basin solar still [15,16], inverted absorber solar still [17–20], tubular solar stills [20–23], solar still coupled with solar collectors, and thermal storage [24–31].

Several factors affect the efficiency of a solar still: the depth of water in the basin, the structure of the solar still, the surface area of the glass and the surface area of the basin, the material, the color, the insulation used, wind velocity, solar radiation, absorbing area, water temperature, cooling systems, inclination angle of the glass, inlet-water temperature, inlet-glass temperature, type of water, and ambient temperature. With various enhancement strategies utilized until now in the literature, the percent improvement in water production achieved varied between 14.7% and 250.3%. Most of the studies available in the literature focused on understanding the effect of these parameters either by experiments or numerical or both. Very few experimental studies exist that used refraction-based sunlight concentration such as embedded convex lenses [27] into the glass cover of a single-basin single-slope solar still or using a line focused Fresnel lens (FRL) [28–31] for improving the productivity of a still. It was found from these articles that enhancement of solar insolation using these techniques could aid in improving the productivity of the still. To design and optimize a typical solar still system, many researchers performed theoretical and numerical analysis. A summary of theoretical analyses performed for different solar still systems are shown in Table 1.

Table 1. Existing theoretical analyses for different configurations of solar stills.

Reference	Model Studied
[32]	Single-sloped basin still with enhanced evaporation and a built-in additional condenser
[33]	Solar still with cooling water flowing between a double-glass cover
[34]	Developed an analytical simulation method of energy behavior of solar stills with varying climatic data and operating conditions
[35]	Studied both passive and active solar stills for different Indian climatic conditions
[36]	Derived an analytical expression for the thermal efficiency for open- and closed-cycle systems of floating tilted wick solar stills
[37]	Derived expressions for water and glass temperatures, yield, and efficiency of both single and double-slope multi-wick solar distillation systems.
[38]	Conducted a seasonal performance analysis for six different water depths in a single-slope passive solar still of cover inclination of 30°.
[39]	Derived correlations to illustrate the effect of solar radiation, dyes, cover slope, and brine depth on the productivity of the basin type solar still.
[40]	Presented a theoretical analysis of a tilted-wick solar still with an inclined flat plate external reflector.
[41]	Presented a numerical study of a passive solar still with separate condenser.
[42,43]	Studied the performance of solar still of a hybrid photovoltaic/ thermal (PV/T) system
[26]	Presented review of numerical as well as experimental investigations on basic types of solar still.
[44]	Compared several numerical models for the estimation of water production from a solar water distillation device.
[45]	Reviewed different methods to improve the effectiveness of the inclined solar still by different researchers and compared their performance.
[46]	Presented a computer simulation model for studying the unsteady-state thermal performance of a single tilted solar powered still.
[47]	Examined three different correlations for heat transfer coefficients available in the literature in order to compare theoretical results with experimental work in terms of hourly yield.

Recently, the authors performed an experimental study using a large-sized, point-focused Fresnel lens (FRL) with a conventional solar still system, for the first time, to enhance the system performance and an improvement of 467.4% in the water productivity rate was observed [48]. In this study, a theoretical model was developed that was used to simulate the solar still system used in the experimental study. Though several still configurations were studied numerically, as shown in Table 1, there are no theoretical models that included the effect of using the FRL in the models and the development of such a model can enable designing high-efficient solar still systems. In this study, the glass temperature, water temperature, and productivity of the still with and without a point-focused FRL were calculated, and the difference in the temperatures and productivity were used to validate the model. Later, the developed model was used to simulate the effect of water depth on the performance of a generic solar still with and without the FRL. Effect of water depth on the performance of the single-slope solar still was studied by a few researchers, e.g., References [9,49–52]. None of the numerical models until now studied the effect of the point-focused refraction-based solar enhancement. A comparison of the tested solar system in terms of cost is also presented.

2. Experiments

The numerical model was validated with experiments in Reference [48]. A single-slope solar still was tested on the main campus of New Mexico State University in Las Cruces, NM, the United States, where the daily max temperature can easily exceed 37.8 °C (100 °F) during the month of June. The solar still was tested during summer climatic conditions to estimate the maximum yields. The experiments were conducted in an open space (32.28° N, 106.75° E) without solar obstruction.

Figure 1 shows the fabricated solar still. The solar still basin (0.45 m × 0.45 m or approximately 0.2 m^2) was made of galvanized steel sheet with a thickness of 2.5 mm. The interior surface of the water basin was painted in black to increase the solar absorptivity. The basin is contained in a 15 mm thick wooden box, of which the shorter and taller sides are about 300 mm and 550 mm, respectively. The space between the basin and the wooden box was filled with a 100 mm thick glass wool board as a thermal insulating layer to reduce heat loss to the ambient. Iron pipes were used as inlet and outlet channels. A metal valve was installed and kept closed during the tests for preventing hot steam leakage through the inlet channel. A piece of tempered glass (0.45 m × 0.52 m) was used as a transparent cover with an inclination of approximately 30°. An electric fan was used to provide forced air flowing parallel to the glass cover. The distillate collection channel was connected to an outlet channel for the measurement of water production by a graduated cylinder. To obtain a good sealing condition, rubber strips were placed between the glass cover and the water basin with wing nuts and washers used to squeeze the rubber strips and the tempered glass. A blow-off valve was installed under the basin bottom to facilitate clean operation.

Figure 1. Solar Still: Basin and Insulation.

The box is surrounded by insulation with the purpose of minimizing heat loss through walls. The insulation material is R18 and is inside a wooden frame (0.1016 m bigger than the basin). The dimensions of the FRL are 0.508 m × 0.559 m × 0.003 m. FRL as shown in Figure 2 helps to focus sunlight through the tempered glass into the basin. The Fresnel lens can be rotated between the wooden arms to move the focal point to the bottom of the basin.

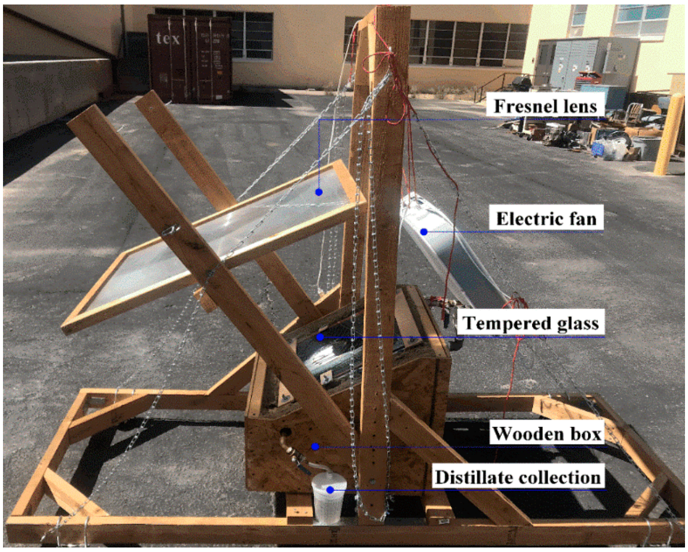

Figure 2. Fresnel lens enhanced solar still.

Each experiment was performed for 13 h, from 9:00 a.m. to 10:00 p.m. in June 2018. FRL was in effect from 9:00 a.m. up to 5:00 p.m., after which the FRL was removed from the wooden swing arms because the sun was too low to use the lens. Four nails were perpendicularly fixed on the two perpendicular surfaces of each swing arm. By observing the nail shadows, the system orientation was adjusted every half-hour such that the glass cover faced the sun, and the concentrated sunlight was refracted to the basin bottom (FRL plane was perpendicular to the incident sunlight). During both the tests, the temperature was recorded every 30 min at different locations in the system e.g., T_a, T_w, T_{gi}, T_{go}. Four calibrated K-type thermocouples were connected to a digital indicator for direct temperature readings. In addition, solar radiation (W/m^2), forced air speed (m/s), and distilled water output (mL) were also measured at the same frequency by using a solar power meter, a portable anemometer and a graduated cylinder, respectively. After each data acquisition, the same amount of saline water was injected into the still to maintain a constant d_w and the desired sodium chloride concentration (30 g/L, to simulate an average salinity of seawater) in the basin. It should be mentioned that the solar radiation on the tempered glass plane (ITG) was measured on the plane parallel with the tempered glass plane without any shading effect from the FRL. After 5:00 p.m., the solar radiation on the FRL plane (IFRL) was measured on the end surface of the wooden swing arm, which was perpendicular to the incident sunlight. To consider the footprint of the solar still, the tested volume of purified water was divided by the basin area (0.2 m^2) in the related figures of the following sections.

K-type thermocouples were placed on different locations inside the solar still to measure temperatures of the water, the inner glass surface, and outer glass surface. One of them was placed outside the solar still to measure the ambient temperature. Temperature, wind speed, and solar radiation data were taken every hour. Excel spreadsheets were used to collect all the data obtained from the experiments. Water temperature, glass temperature, wind speed, fan speed, and solar intensity were taken using a solar power meter, an anemometer and a K-type thermometer.

3. Numerical Model

Though numerous experimental investigations are reported in the literature on better design for solar stills, the experimental investigations can be expensive, laborious, and time-consuming. Hence, mathematical modeling is an attractive alternative to investigate and develop better designs for solar stills under various operational parameters. The present model employed equations developed by

Dunkle in Reference [52–54] and were analyzed using a MATLAB code and EXCEL spreadsheets. Various assumptions were made to simplify the analysis:

- In the still, there is no vapor leakage.
- Compared to the heat capacity of the basin water, the heat capacity of insulating materials used in the solar still is negligible.
- The physical water properties remain constant even with different temperatures.

Figure 3 shows the different heat transfer process that occurs in a solar still. It is easier to evaluate the heat transfer distribution in the still and the temperature rates if the solar still analysis is divided into parts such as basin, glass, and basin water, as well as internal heat transfer and external heat transfer processes [55–60]. The next few subsections briefly describe the equations used for the current model.

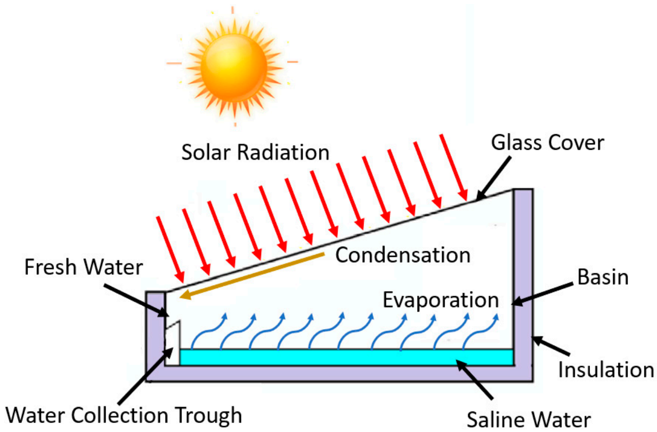

Figure 3. Heat transfer process in a solar still.

3.1. Internal Heat Transfer

The heat transfer generated inside the solar still is considered as internal heat transfer that is responsible for the evaporation process to produce water vapor from impure water, producing fresh water. It is the exchange of heat between water and the inner glass surface, which can be divided into convection, evaporation, and radiation [61–68].

The mathematical model is expressed in terms of water temperature T_w, internal glass temperature T_{gi}, and basin temperature, T_{bi}. Initial glass temperature, initial basin temperature, and initial water temperature are provided as input parameters. Partial vapor pressure, P_g, and water pressure, P_w, in a still can be obtained using the following equations, Reference [52–54]:

$$P_w = \exp\left(25.317 - \frac{5144}{T_{wi} + 273}\right) \tag{1}$$

$$P_g = \exp\left(25.317 - \frac{5144}{T_{gi} + 273}\right) \tag{2}$$

Natural convection takes place because of the temperature difference between the water and the inner surface of the glass. The rate of convective heat transfer, Q_{Cwgi}, and the heat transfer coefficient, h_{Cwgi}, between water and the inner glass surface are expressed as:

$$Q_{Cwgi} = h_{Cwgi} \times \left(T_w - T_{gi}\right) \tag{3}$$

$$h_{Cwgi} = 0.884\left[\left(T_w - T_{gi}\right) + \frac{\left(P_w - P_g\right)(T_w + 273)}{268,900 - P_w}\right]^{1/3} \tag{4}$$

Evaporation heat transfer occurs between water mass and the inner glass surface and is generated when the vapor pressure is lower than the saturation pressure of the liquid. Evaporation heat transfer, Q_{Ewgi}, and heat transfer coefficient, h_{Ewgi}, are calculated as:

$$Q_{Ewgi} = h_{Ewgi} \times \left(T_w - T_{gi}\right) \tag{5}$$

$$h_{Ewgi} = 16.28 \times 10^{-3} \times h_{Cwgi} \left(\frac{\left(P_w - P_g\right)}{\left(T_w + T_{gi}\right)} \right) \tag{6}$$

Radiation heat transfer is produced by the emission of internal energy between two bodies having different temperatures which are, in this case, water mass and the inner glass surface. Radiation heat transfer and heat transfer coefficient are expressed as:

$$Q_{Rwgi} = h_{Rwgi} \times \left(T_w - T_{gi}\right) \tag{7}$$

$$h_{Rwgi} = \varepsilon_{eff} \sigma \frac{\left[(T_w + 273)^4 - \left(T_g + 273\right)^4\right]}{\left(T_w - T_{gi}\right)} \tag{8}$$

In Equation (8), σ is the Stefan Boltzmann's constant taken as 5.67×10^{-8} W/m^2 K^4, ε_{eff} is the effective emissivity between water mass and the glass cover which depends on the emissivity of water (ε_w) and emissivity of glass (ε_g) and is given by the following expression:

$$\varepsilon_{eff} = \left(\frac{1}{\varepsilon_w} + \frac{1}{\varepsilon_g} - 1 \right)^{-1} \tag{9}$$

The summation of convection, radiation, and evaporation rates provide the total internal heat transfer rate, Q_{Twgi}, and the total internal heat transfer coefficient, h_{Twgi}, is expressed as:

$$Q_{Twgi} = Q_{Cwgi} + Q_{Ewgi} + Q_{Rwgi} \tag{10}$$

$$h_{Twgi} = h_{Cwgi} + h_{Ewgi} + h_{Rwgi} \tag{11}$$

3.2. External Heat Transfer

External heat transfer is the heat loss from the solar still and occurs between the basin of the still and the surroundings. The total external heat loss can be divided into the top heat loss, bottom heat loss, and side heat loss [57–62]. The upper heat loss is the heat loss from the outer glass cover to the atmosphere due to radiation and convection heat transfer [62–68]. The convection heat transfer loss, Q_{Cgoa} from the outer glass cover to the atmosphere, can be defined by:

$$Q_{Cgoa} = h_{Cgoa}\left(T_g - T_a\right) \tag{12}$$

$$\begin{aligned} h_{Cgoa} &= 2.8 + 3.0 \times v_w, \text{ if wind velocity, } v_w \le 5 \text{ m/s} \\ h_{Cgoa} &= 2.8 + 3.8 \times v_w, \text{ if wind velocity, } v_w > 5 \text{ m/s} \end{aligned} \tag{13}$$

The convection heat transfer coefficient, h_{Cgoa}, depends on the wind speed, as shown in Equation (13). The radiation heat transfer coefficient, h_{Rgoa}, is the heat loss from the outer glass cover to the atmosphere due to radiation and can be obtained by:

$$h_{Rgoa} = \varepsilon_{eff} \sigma \frac{\left[\left(T_{go} + 273\right)^4 - \left(T_{sky} + 273\right)^4\right]}{\left(T_{go} - T_{sky}\right)} \tag{14}$$

where, T_{go} is the outer glass temperature and T_{sky} is the sky temperature, expressed in terms of ambient temperature, T_a, as:

$$T_{sky} = 0.0552 \times T_a{}^{1.5} \tag{15}$$

The total upper heat loss coefficient, h_{Tgoa}, between the outer glass cover and the surroundings is described as:

$$h_{Tgoa} = h_{Cgoa} + h_{Rgoa} \tag{16}$$

The sum of the radiative heat loss and the convective heat loss is equal to the total upper heat loss, Q_{Tgoa}, and is calculated by:

$$Q_{Tgoa} = Q_{Cgoa} + Q_{Rgoa} \tag{17}$$

To calculate the overall heat loss coefficient, U_{Tgia}, from the inner glass cover to the atmosphere, the following equation can be used:

$$U_{Tgia} = \frac{\frac{K_g}{L_g} \times h_{Tgoa}}{\frac{K_g}{L_g} + h_{Tgoa}} \tag{18}$$

The overall heat loss coefficient is used to obtain the overall heat loss coefficient, U_T, from the top glass cover, which is expressed as:

$$U_T = \frac{h_{Twgi} \times U_{Tgia}}{hT_{wgi} + U_{Tgia}} \tag{19}$$

The heat loss is transferred from the basin to the atmosphere through the walls of the basin and the insulation due to convection, conduction, and radiation. The rate of convective heat transfer between the basin and the water mass, Q_w, can be obtained as:

$$Q_w = h_w(T_b - T_w) \tag{20}$$

where, h_w is the heat transfer between the basin liner and the water. The rate of conduction heat transfer between the basin and the surroundings (Q_b) is obtained by:

$$Q_b = h_b(T_b - T_a). \tag{21}$$

In Equation (21), A_b is the basin area that is exposed to water. The conduction heat transfer coefficient between the basin and the surroundings, h_b, with insulation, is expressed as:

$$h_b = \left(\frac{L_i}{K_i} + \frac{1}{h_{Tba}}\right)^{-1} \tag{22}$$

where, h_{Tba} is the total heat transfer coefficient that considers the effect of both the free convection and radiation:

$$h_{Tba} = 5.7 + (3.8 \times v_w) \tag{23}$$

If no insulation is present, then, h_b is equal to h_{Tba}. The overall bottom heat transfer coefficient between the water mass and the surroundings is given by:

$$U_b = \frac{h_w \times h_b}{h_w + h_b} \tag{24}$$

The overall side heat transfer coefficient, U_{ss}, between the water and the surroundings is obtained by:

$$U_{ss} = \left(\frac{A_{ss}}{A_b}\right) U_b \tag{25}$$

where, A_{ss} is the total area of the solar still, and A_b is the basin area that is exposed to water on the sides. Therefore, the total heat transfer coefficient from the basin to the surroundings is the sum of the overall middle heat transfer coefficient and the overall lower heat coefficient between the water and the surroundings:

$$U_{bs} = U_b + U_s \tag{26}$$

The overall external heat transfer loss coefficient from the top, bottom, and sides is expressed as:

$$U_{Ls} = U_t + U_{bs} \tag{27}$$

3.3. Temperatures and Productivity

The hourly productivity in a solar still can be calculated by:

$$m_w = \frac{QE_{wgi}}{L_{ev}} \tag{28}$$

The daily productivity in the solar still can then be obtained as follows:

$$M_w = \sum_{i=1}^{24} m_w \tag{29}$$

Based on the above equations, the inner glass temperature, T_{gi}, basin temperature, T_b, and water temperature, T_w, over time are estimated as follows after applying the energy balance equations:

$$T_w = \frac{f(t)}{a}\left(1 - e^{-at}\right) + T_w(i)e^{-at} \tag{30}$$

where,

$$a = \frac{U_{LS}}{m_w \times C_{pw}} \tag{31}$$

and,

$$f(t) = \frac{\alpha_{eff} \times I(t) + U_{LS} \times T_a}{m_w \times C_w} \tag{32}$$

In Equation (32), α_{eff} is the effective absorptivity and is calculated as:

$$\alpha_{eff} = \alpha'_b \times \frac{h_w}{h_w + h_b} + \alpha'_w + \alpha'_g \times \frac{hT_{wgi}}{hT_{wgi} + hT_{goa}} \tag{33}$$

In the above equation, α'_b, α'_w, and α'_g, are the fraction of solar flux absorbed by basin liner, basin water, and glass cover, respectively. These are calculated as:

$$\alpha'_b = \alpha_b \times \left(1 - \alpha_g\right)\left(1 - R_g\right)(1 - R_w) \times \left[\sum \mu_j EXP\left(\eta_j d_w\right)\right] \tag{34}$$

$$\alpha'_w = \alpha_w \left(1 - \alpha_g\right)\left(1 - R_g\right)(1 - R_w) \times \left[1 - \sum \mu_j EXP\left(\eta_j d_w\right)\right]. \tag{35}$$

$$\alpha'_g = \left(1 - R_g\right)\alpha_g \tag{36}$$

where, $(\sum \mu_j EXP(\eta_j d_w))$ is the attenuation factor and depends on different lengths, as shown in Table 2. R_g and R_w are the reflectivities of glass cover and water, respectively [31]. *I(t)* is the insolation over time.

The inner glass temperature, T_{gi}, and basin temperature, T_b, are given by the following equations:

$$T_{gi} = \frac{\alpha'_g I(t) + h_{Twgi} \times T_w + U_{Tgia} \times T_a}{h_{Twgi} + U_{Tgia}} \tag{37}$$

$$T_b = \frac{\alpha'_b I(t) + h_w \times T_w + h_b \times T_b}{h_w + h_b} \tag{38}$$

To account for the presence of FRL in the model developed, the insolation, *I(t),* was replaced by $I_{eff}(t)$, which is estimated using the following equation:

$$I_{eff}(t) \;=\; I(t) \;\times A_{FRL}/A_G \times \tau_{FRL} \tag{39}$$

Equation (39) assumes that all the radiation that is incident on the FRL is concentrated onto the solar still glass, and hence the overall incident energy onto the solar still increased by a factor of concentration ratio: A_{FRL}/A_G. It should be noted that optical losses are neglected in the above equation. A mathematical model was developed using the above set of equations, and was used to predict the glass temperature, water temperature, convection, radiation and evaporation heat transfer, heat loss transfer inside and outside the solar still, hourly productivity and daily productivity, with respect to solar intensity, wind velocity, and time using EXCEL and MATLAB software.

Table 2. Attenuation (Att.) Factors for varying water depth, Reference [31].

d_w (m)	Att. Factor
0.02	0.6756
0.03	0.6441
0.04	0.6185
0.05	0.6124
0.06	0.5858
0.08	0.5648
0.10	0.5492

4. Results

4.1. Experimental Results with and without Fresnel Lens (FRL)

Table 3 shows the insolation and ambient temperature encountered during the experiments without and with FRL. It can be observed that both insolation and ambient temperature were slightly different on both days. The heat concentrated on to the bottom of the still is distributed into the basin and water and result in the temperature rise of water. It can be observed that the maximum insolation (1085 W/m^2 with no FRL and 1085 W/m^2 with FRL) is observed around 2 p.m. and the ambient temperature is also maximum at the same time. Figure 4 shows the water and glass temperatures measured during the experiments.

The maximum temperatures of water and glass are around times of higher maximum solar intensity. It can also be observed that when a FRL was used, both the water temperature and glass temperature are much higher when compared to this temperature when no FRL was used. The maximum T_w and T_g observed with no FRL case are 59.4 °C and 55.7 °C respectively, whereas, with FRL case, they are 87.6 °C and 79.4 °C, respectively. Figure 5 shows the cumulative water output or cumulative productivity measured during both the experiments. The total productivity in the case of FRL (8.324 kg/m^2) is around 6.38 times higher than the productivity achieved in case of no FRL (1.303 kg/m^2). This clearly shows that utilizing an external heat transfer mechanism can enhance the heat input and can significantly improve the performance or productivity of a still.

Table 3. Hourly variation of solar intensities, and ambient temperatures for experiments with and without FRL.

Time (Hours)	No FRL (Day 1)		With FRL (Day 2)	
	Insolation (W/m^2)	T_{amb} (°C)	Insolation (W/m^2)	T_{amb} (°C)
9:00	513	27.5	502	27.5
10:00	674	29.5	670	29.4
11:00	872	32.8	874	33.3
12:00	1027	36.6	1021	36.6
13:00	1083	39.6	1078	39.4
14:00	1085	41.1	1084	41.3
15:00	983	41.2	964	41.2
16:00	832	41.6	836	40.9
17:00	615	40.8	606	40.8

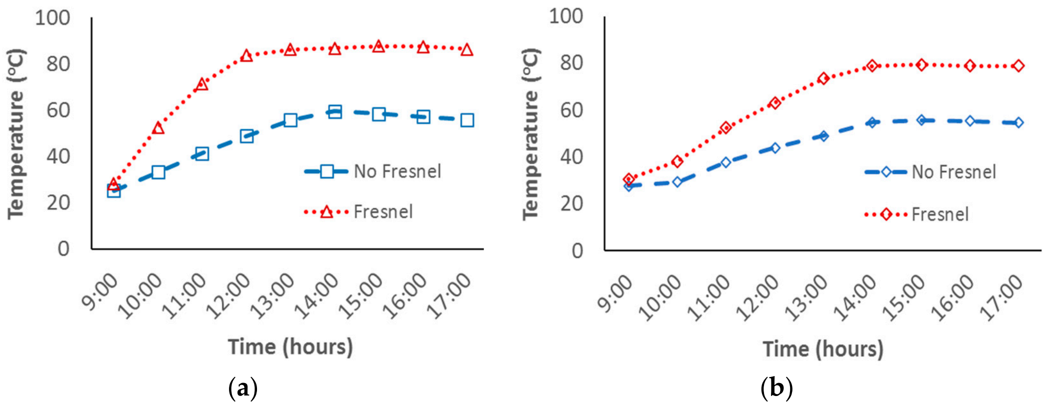

Figure 4. The measured temperatures during experiments (**a**) water temperature, (**b**) glass temperature.

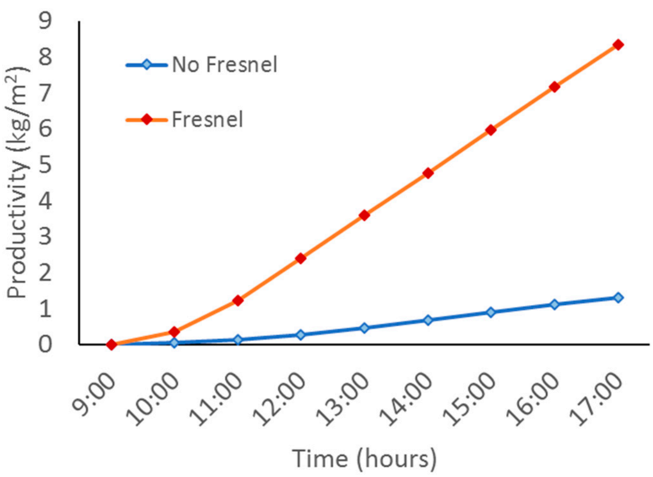

Figure 5. Cumulative water productivity.

4.2. Comparison of the Numerical Model with Experiments

The developed model was used to simulate the parameters of the still used in the experiments. Table 4 shows the physical input parameters for the model. In our experiments, a fan was used to maintain forced convection on the glass. Hence, the wind velocity of 4.2 m/s was used at all times. A smooth curve for ambient temperature was used in the numerical model to eliminate the sudden changes in temperature and hence, all other factors estimated.

Table 4. Parameters used for validating the experiments.

Parameters	Numerical Values Used for Validation
Basin area, A_b	0.2025 m^2
Basin absorptivity, α_b	0.90
Glass absorptivity, α_g	0.05
Water reflectivity, α_w	0.05
Glass reflectivity, R_g	0.05
Water reflectivity, R_w	0.05
Glass emissivity, ε_g	0.94
Water emissivity, ε_w	0.95
Water heat capacity, c_w	4180 J/kg K
Time, t	3600 s
The thickness of glass cover, L_g	0.004 m
The thickness of insulation, L_i	0.1016 m
Glass thermal conductivity, k_g	1.03 W/m K
Insulation thermal conductivity, k_i	0.0363 W/m K
σ	5.6697×10^{-8} W/m^2 K^4
h_w	250 W/m^2 K
Water density, ρ_w	1000 kg/m^3
Water depth, d	0.02 m
Wind velocity with fan	4.2 m/s
Concentration ratio, A_{FRL}/A_G	3.237
Glass Transmissivity, τ_g	0.88
FRL Transmissivity, τ_{FRL}	0.88

Figures 6 and 7 show the comparison of a numerical model with experiments. It can be observed that the current model predicts experimental results well. The average difference between the experiments and numerical model was found to be 4% for water temperature and 9% for glass temperature for the case with no FRL. The average difference between the experiments and numerical model was found to be 4% for water temperature and 5% for glass temperature when the FRL was used. It should be noted that the model assumes all the heat transmitted from the FRL is concentrated onto the still, and hence no optical or heat loss from FRL to still is accounted for.

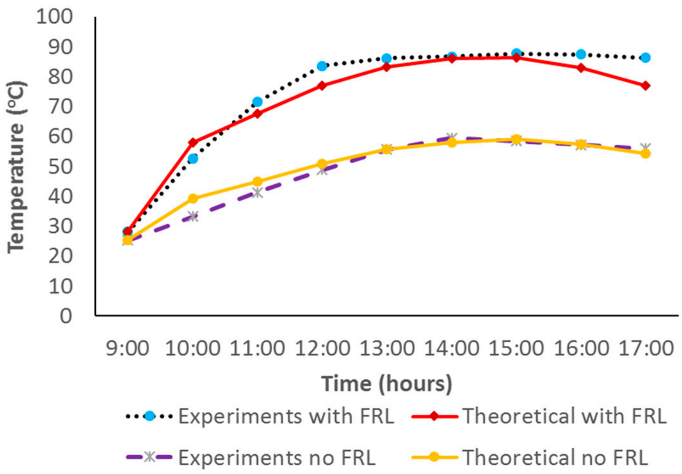

Figure 6. Hourly variation of experimental and theoretical values of water temperatures.

The cumulative water productivity observed in the experiments and theoretical model for the time period 9:00 a.m. to 5:00 p.m. is shown in Table 5. The theoretical model was used to include only the time period when the FRL is active.

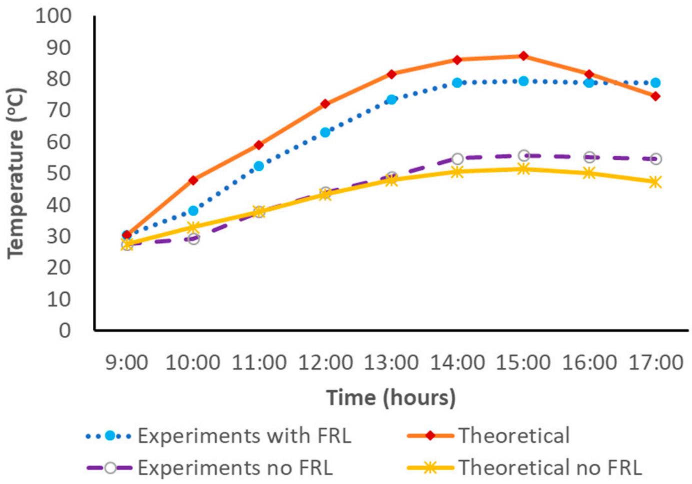

Figure 7. Hourly variation of experimental and theoretical values of glass temperatures.

Table 5. Cumulative water productivity comparison between experiments and theoretical model.

Time Period Used for the Model	Productivity No FRL		Productivity with FRL	
	Theoretical (Kg/m^2)	Experimental (Kg/m^2)	Theoretical (Kg/m^2)	Experimental (Kg/m^2)
9 a.m.–5 p.m.	1.788	1.303	8.127	8.324

It could be observed from Figures 6 and 7 that the temperatures in the theoretical model follow the same trend as the experimental results. Once the numerical model is validated, a parametric study was performed to understand the effect of FRL when varying water depths are used.

4.3. Impact of FRL on Varying Water Depths

The parametric study assumed that the water depth varied from 2 cm to 10 cm. The model was used to simulate the performance of a still used in Reference [31]. This still was chosen for the study since experiments were performed in Reference [31] for varying depths without a FRL. The insolation, ambient temperatures, and parameters that were changed for the parametric study are shown in Tables 6 and 7.

Table 6. Solar insolation and ambient temperatures used for the parametric study.

Time (Hours)	Insolation (W/m^2)	T_{amb} (°C)
9:00	731	33.9
10:00	852	35.6
11:00	909	37.1
12:00	911	38.3
13:00	860	39.1
14:00	770	39.7
15:00	599	40
16:00	360	39.9
17:00	121	39.6

Figure 8 shows the hourly cumulative productivity obtained for different depths. The maximum productivity is obtained from lower basin water depth (2 cm) and minimum for higher basin water depth (10 cm). It can be observed that the productivity decreases with increase in depth for both no FRL and FRL cases. This is caused by the higher rate of evaporation for lower basin depth compared to higher depths due to higher temperature rise.

Table 7. Modified still parameters used for parametric study.

Parameters	Numerical Values Used for Parametric Study
A_b	1 m^2
L_i	0.010 m
k_i	0.033 W/m K
d_w	0.02 m, 0.04 m, 0.06 m, 0.08 m, 0.09 m, 0.10 m

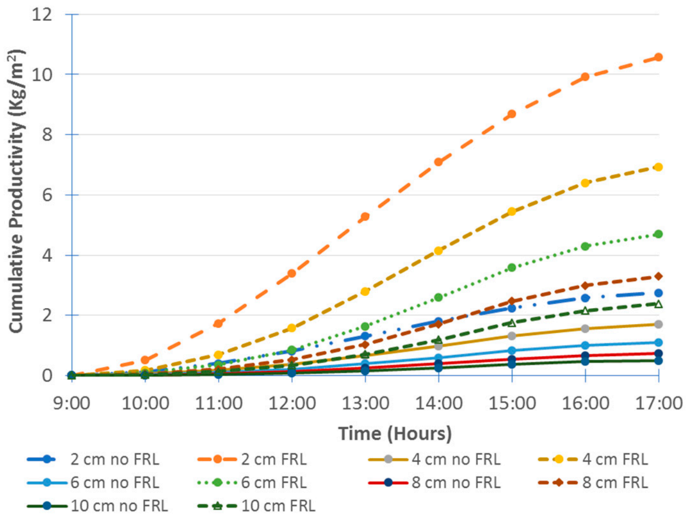

Figure 8. Hourly variation of cumulative water productivity with and without FRL for different depths.

The total productivity of the still with and without FRL obtained in the parametric study is shown in Table 8. It can be observed that productivity decreased as the water depth increased. In similar studies with single-basin single-slope solar stills (without FRL), the water productivity was found to range from 2.1 kg/m^2/day to 5.5 kg/m^2/day depending on the location, size of the still, and whether the attenuation factor was considered or not in the theoretical analysis, e.g., References [9,49–52]. In addition, as observed in the current study, it was found in earlier studies that decrease in water depth enhanced the productivity rate. When productivity with and without FRL is compared in Table 8, it can be observed that the percent increase in productivity also improves when the water depth is increased. Also, the productivity value with FRL at 9 cm is almost equal to the productivity of still with no FRL at 2 cm depth (Figure 9). From this observation, it can be concluded that by utilizing a FRL, the initial mass of water can be higher (almost 4.5 times in the present case) to get the same productivity. This could enable the advantage of less frequent replenishment of water.

Table 8. Predicted productivity with and without FRL for varying water depths.

Depth	Productivity No FRL (Kg/m^2)	Productivity with FRL (Kg/m^2)	% Increase with FRL *
2 cm	2.755	10.573	383.8
4 cm	1.697	6.936	408.8
6 cm	1.101	4.695	426.3
8 cm	0.744	3.292	442.5
9 cm	0.614	2.791	454.6
10 cm	0.505	2.384	472.2

* increased productivity is due to the increased heat input per m^2 of the still as per the concentration ratio, not to be confused with thermal efficiency.

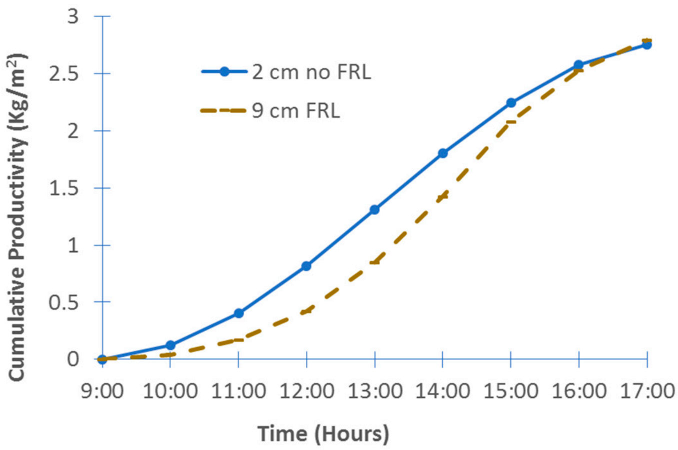

Figure 9. Hourly variation of cumulative productivity for 2 cm without FRL and 2 cm with FRL.

4.4. Thermal Efficiency of the Still

The thermal efficiency of the still with both the FRL and no FRL cases for all the depths was calculated using Equation (40). The efficiency was calculated using two different assumptions. One by considering the attenuation factor which showed low theoretical water output and hence lower efficiency.

$$\eta = \frac{M_w \times L_{ev}}{A_b \times \sum I(t) \times \Delta \mathrm{t}} \tag{40}$$

Figure 10 shows the obtained thermal efficiency of the still for all the depths with and without considering the attenuation factors. While using the attenuation factor in the code provided much better comparison with the water and glass temperatures, it was found that not using the attenuation factor predicted higher productivity of the still. This was also noticed in previous studies in the literature e.g., in Reference [52]. Hence, the results shown in the figure can be interpreted qualitatively rather than quantitatively to observe the effect of FRL. It can be observed from Figure 9 that the use of the FRL also improves the thermal efficiency of the still for the parameters considered in the study.

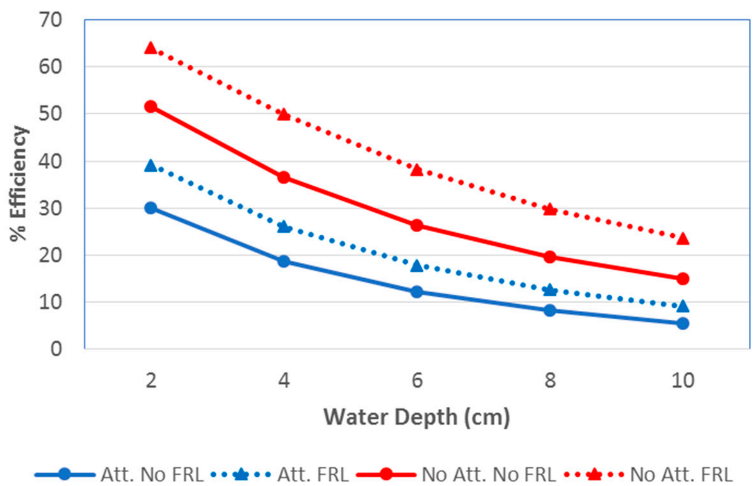

Figure 10. Theoretical efficiencies for different depths with and without using attenuation factor (Att.).

4.5. Economic Performance

The economic performance of the solar still system that was used in experiments was evaluated by calculating the cost of purified water per liter (χ_{CPL}). In principal, χ_{CPL} depends on the annual fixed cost (χ_{AFC}), the annual cost on system maintenance and operation (χ_{AMC}), the annual salvage value (χ_{ASV}) and the annual fresh water yield (m_{water}), as indicated by the following equation [69]:

$$\chi_{\mathrm{CPL}} = \frac{\chi_{\mathrm{AFC}} + \chi_{\mathrm{AMC}} - \chi_{\mathrm{ASV}}}{m_{\mathrm{water}}} \tag{41}$$

Here, χ_{AFC} was obtained by using the following relationship:

$$\chi_{\mathrm{AFC}} = \kappa \times \chi_{\mathrm{FC}} \tag{42}$$

where, χ_{FC} and κ stand for the fixed cost and the recovery factor, respectively. In the present work, the χ_{FC} for the system with the Fresnel lens was approximately equal to \$325, whereas the χ_{FC} for the system without the Fresnel lens was about \$199. κ can be determined by using the following equation:

$$\kappa = \frac{i \times (i+1)^n}{(i+1)^n - 1} \tag{43}$$

where, the interest per year (i) and system life year (n) were considered in this study to be 3% and 10 years, respectively. χ_{AMC}, which mainly includes the costs in regular water filling, fresh water collecting, and cleaning of the system, was assumed to be 30% of χ_{AFC}. The annual salvage value (χ_{ASV}) can be calculated by multiplying the salvage value (χ_{sv}) by sink fund factor (μ), as shown by Equation (4):

$$\chi_{\mathrm{ASV}} = \mu \times \chi_{\mathrm{SV}} \tag{44}$$

where, χ_{SV} was thought to account for about 20% of χ_{FC}. Meanwhile, μ was obtained by using the following equation:

$$\mu = \frac{i}{(i+1)^n - 1} \tag{45}$$

In Equation (41), m_{water} means the sum of the system daily yield throughout an entire year. However, the system daily yield varies with respect to season, weather condition, operation parameter, etc., consequently making it impossible to accurately calculate the m_{water}. Therefore, approximations concerning m_{water} have been adopted by researchers in the field of solar still. For example, Pakdel et al. multiplied the highest system daily yield by the number of operation days to get m_{water} [70]. In contrast, Haddad et al. used an averaged system daily yield, which was obtained by considering the test results of different seasons [71]. In the current study, the method in Reference [70] was adopted, because the proposed solar still system was only tested during the summer season. Thus, the system daily yields with the Fresnel lens and without the Fresnel lens were considered 1.625 L/m^2 and 9.22 L/m^2 respectively, as experimentally measured in Section 3.1. By assuming that desalination systems operate for 340 days in a year, the m_{water}s were calculated to be 552.5 L/m^2 and 3134.8 L/m^2, respectively. By substituting the obtained m_{water}s into Equation (41), the economic analysis was finalized, as summarized in Table 9. It is obvious that although the introduction of the Fresnel lens increased χ_{FC} and thus both χ_{AFC} and χ_{AMC}, the calculated χ_{CPL} decreased due to the significant increase in m_{water}. It should be noted that we did not include the cost of an automatic tracking system that keeps the lens in the correct position and the system in the right alignment, which might add costs.

Table 9. Cost of solar still configurations with and without FRL used in experiments [48].

Different Configurations	m_{water} (L/m^2)	χ_{FC} (\$)	χ_{AFC} (\$)	χ_{ASV} (\$)	χ_{AMC} (\$)	χ_{CPL} (\$/(L-m^2))
Without Fresnel lens	552.5	199	23.3	3.47	6.99	0.049
With Fresnel lens	3134.8	325	38.1	5.67	11.43	0.014

5. Conclusions

This work presents the performance of a solar still when an external FRL was used to increase the effective solar heat input. The study shows that utilizing a FRL results in increased water and glass temperatures and can significantly improve the productivity of the still. Productivity of 638% improvement was observed in the experiments performed. The water depth was varied between 2 cm and 10 cm for the parametric study. It was observed that the percent improvement in productivity increases with increased water depth. In addition, the thermal efficiency of the still also improved when FRL is used. In conclusion, the results show that utilizing the FRL can significantly aid in improving the productivity of the still, which would be beneficial especially in remote areas. Future improvements could be made by using a tracking mechanism for much better focusing of the FRL into the still, scale-up analysis, depending on the location and requirements.

Author Contributions: Software, A.J., and S.K.; validation, L.M., Y.H.P., and H.W.; formal analysis, K.K., and S.K.; resources, D.J.V.; writing—original draft preparation, A.J., and S.K.; writing—review and editing, K.K., D.J.V., Y.H.P., and P.X.; funding acquisition, S.K., D.J.V., Y.H.P., K.K., P.X., and H.W.

Funding: This research project is supported by the New Mexico Water Resources Research Institute and the US Bureau of Reclamation through a cooperative agreement. This study was also supported in part by the Wheels of Change Program Grant no. 2015-38422-24112 and I-DISCOVER Program Grant no. 2014-38422-22078 from the USDA National Institute of Food and Agriculture.

Conflicts of Interest: The authors declare no conflict of interest.

Nomenclature

A_{FRL}	Area of the Fresnel lens (m^2)
A_G	Area of glass cover exposed to solar radiation (m^2)
A_w	Water basin area (m^2)
A_{ss}	Area of sidewalls (m^2)
C_{pw}	Water specific heat (kJ/kg K)
FRL	Fresnel lens
h_b	Heat transfer coefficient basin and ambient (W/m^2 K)
hC_{wgi}	Conductive heat transfer coefficient from glass inner surface to glass outer surface (W/m^2 K)
hC_{goa}	Convective heat transfer coefficient from glass cover outer surface to ambient (W/m^2 K)
hE_{wgi}	Evaporative heat transfer coefficient from water and inner surface of the glass cover (W/m^2 K)
hR_{ba}	Radiation heat transfer coefficient from basin to ambient (W/m^2 K)
hR_{goa}	Radiation heat transfer coefficient from cover outer surface to ambient (W/m^2 K)
hR_{wgi}	Radiation heat transfer coefficient from water to glass cover inner surface (W/m^2 K)
hT_{goa}	Total top heat loss coefficient between cover outer surface and atmphere (W/m^2 K)
h_w	Convective heat trafer coefficient between basin liner and water mass (W/m^2 K)
hT_{wgi}	Total heat transfer coefficient from water to glass cover inner surface (W/m^2 K)
$I(t)$	Intensity of solar radiation (W/m^2)
$I_{eff}(t)$	Effective Solar Intensity with Fresnel lens (W/m^2)
K_g	Glass thermal conductivity (W/m K)
K_i	Insulation thermal conductivity (W/m K)
L_g	Glass thickness (m)
L_i	Insulation thickness (m)
L_{ev}	Latent heat of vaporization (kJ/kg)
m_w	Hourly productivity from SS (kg/m^2 h)
M_w	Daily yield from SS (kg/m^2 day)
P_g	Partial vapor pressure (Pa)
P_w	Water pressure (Pa)
Q_b	Heat loss between basin and ambient (W/m^2)
Q_{Cwgi}	Convective heat transfer rate within SS from water to glass cover inner surface (W/m^2)
Q_{Cgoa}	Convective heat transfer rate from glass cover outer surface to ambient (W/m^2 K)
Q_{Rgoa}	Radiative heat transfer rate from glass outer surface to ambient (W/m^2 K)
Q_{Ewgi}	Evaporative heat transfer rate within SS from water to glass cover inner surface (W/m^2)
Q_{Tgoa}	Total radiative and convective heat losses (W/m^2 K)
Q_{Twgi}	Total heat transfer rate from water to glass cover inner surface (W/m^2)

Q_{Rwgi}	Radiative heat transfer rate within SS from water to glass cover inner surface (W/m^2)
Q_u	Rate of thermal feed from external devices to SS (W/m^2)
Q_w	Heat tnsfer rate between basin linear water mass (W/m^2)
R_g	Reflectivity of glass cover
R_w	Reflectivity of basin water
T_a	Ambient temperature (°C)
T_b	Basin temperature (°C)
T_g	Glass cover temperature (°C)
T_{gi}	Glass cover inner surface temperature (°C)
T_{go}	Initial temperature of glass cover (°C)
T_{sky}	Sky temperature (°C)
T_w	Water Temperature (°C)
U_b	Overall bottom heat loss coefficient between water mass and atmosphere (W/m^2 K)
U_{bs}	Total bottom and side heat transfer loss coefficient from water mass to surrounding atmosphere (W/m^2 K)
U_{ls}	Overall external heat transfer loss coefficient from water mass to the surroundings (W/m^2 K)
U_{LS}	Overall heat loss coefficient between water mass and atmosphere (W/m^2 K)
U_T	Overall top heat loss coefficient between water mass and atmosphere (W/m^2 K)
U_{Tgia}	Overall heat loss coefficient from glass cover inner surface to atmosphere (W/m^2 K)
V_w	Wind velocity (m/s)
d	Water depth (m)
Greek Symbols	
ε_{eff}	Effective remittances
σ	Steven Boltzmann constant (W/m^2 K^4)
ε_w	Water emissivity
ε_g	Glass cover emissivity
α_w	Water absorptivity
α_b	Basin absorptivity
α_g	Cover glass absorptivity

References

1. Sangroya, D.; Nayak, J.K. Development of wind energy in India. *Int. J. Renew. Energy Res.* **2015**, *5*, 1–13.
2. Sengar, S.H.; Khandetod, Y.P.; Mohod, A.G. New innovation of low cost solar still. *Eur. J. Sustain. Dev.* **2012**, *1*, 315–352.
3. Fath, H.E. Solar distillation: A promising alternative for water provision with free energy, simple technology and a clean environment. *Desalination* **1998**, *116*, 45–56. [CrossRef]
4. UMAR, S.; Yakubu, A.; Musa, M.; Muhammad, S.B. Experimental Investigation and Performance Analysis of Single Slope Solar Still. *Int. J. Renew. Energy Res.* **2017**, *7*, 1621–1628.
5. Ismail, B.I. Design and performance of a transportable hemispherical solar still. *Renew. Energy* **2009**, *34*, 145–150. [CrossRef]
6. Arunkumar, T.; Vinothkumar, K.; Ahsan, A.; Jayaprakash, R.; Kumar, S. Experimental Study on Various Solar Still Designs. *ISRN Renew. Energy* **2012**, *2012*, 1–10. [CrossRef]
7. Fath, H.; El-Samanoudy, M.; Fahmy, K.; Hassabou, A. Thermal-economic analysis and comparison between pyramid-shaped and single-slope solar still configurations. *Desalination* **2003**, *159*, 69–79. [CrossRef]
8. Al-Karaghouli, A.; Alnaser, W. Experimental comparative study of the performances of single and double basin solar-stills. *Appl. Energy* **2004**, *77*, 317–325. [CrossRef]
9. Yadav, Y. Transient analysis of double-basin solar still integrated with collector. *Desalination* **1989**, *71*, 151–164. [CrossRef]
10. Tiwari, G. Enhancement of daily yield in a double basin solar still. *Energy Convers. Manag.* **1985**, *25*, 49–50. [CrossRef]
11. Bălan, R.; Chandrasekaran, J.; Shanmugan, S.; Janarthanan, B.; Kumar, S. Review on passive solar distillation. *Desalin. Water Treat.* **2011**, *28*, 217–238. [CrossRef]

12. Gnanadason, M.K.; Kumar, P.S.; Sivaraman, G.; Daniel JE, S. Design and performance analysis of a modified vacuum single basin solar still. *Smart Grid Renew. Energy.* **2011**, *2*, 388. [CrossRef]
13. Murugavel, K.K.; Srithar, K. Performance study on basin type double slope solar still with different wick materials and minimum mass of water. *Renew. Energy* **2011**, *36*, 612–620. [CrossRef]
14. El-Sebaii, A. Thermal performance of a triple-basin solar still. *Desalination* **2005**, *174*, 23–37. [CrossRef]
15. Tiwari, G.; Singh, S.; Bhatnagar, V. Analytical thermal modelling of multi-basin solar still. *Energy Convers. Manag.* **1993**, *34*, 1261–1266. [CrossRef]
16. Yamaguchi, Y.; Sato, H. Development of small-scale multi-effect solar still. In Proceedings of theASME 2003 International Solar Energy Conference, Kohala Coast, HI, USA, 15–18 March 2003; pp. 167–173.
17. Suneja, S.; Tiwari, G. Effect of water flow on internal heat transfer solar distillation. *Energy Convers. Manag.* **1999**, *40*, 509–518. [CrossRef]
18. Suneja, S.; Tiwari, G. Effect of water depth on the performance of an inverted absorber double basin solar still. *Energy Convers. Manag.* **1999**, *40*, 1885–1897. [CrossRef]
19. Suneja, S.; Tiwari, G. Parametric study of an inverted absorber triple effect solar still. *Energy Convers. Manag.* **1999**, *40*, 1871–1884. [CrossRef]
20. Suneja, S.; Tiwari, G. Optimization of number of effects for higher yield from an inverted absorber solar still using the Runge-Kutta method. *Desalination* **1998**, *120*, 197–209. [CrossRef]
21. Ahsan, A.; Fukuhara, T. Mass and heat transfer model of Tubular Solar Still. *Sol. Energy* **2010**, *84*, 1147–1156. [CrossRef]
22. Ahsan, A.; Islam, K.M.S.; Fukuhara, T.; Ghazali, A.H. Experimental study on evaporation, condensation and production of a new Tubular Solar Still. *Desalination* **2010**, *260*, 172–179. [CrossRef]
23. Ahsan, A.; Fukuhara, T. Condensation mass transfer in unsaturated humid air inside tubular solar still. *J Hydrosci. Hydraul. Eng.* **2010**, *28*, 31–42.
24. Rajesh, V.R. Performance evaluation of a solar desalination system integrated with a fresnel lens concentrator. *Int. J. Renew. Energy Res.* **2016**, *6*, 250–253.
25. Kuravi, S.; Trahan, J.; Rahman, M.M.; Goswami, D.Y.; Stefanakos, E.K. Analysis of transient heat transfer in a thermal energy storage module. In Proceedings of theASME 2010 International Mechanical Engineering Congress and Exposition. American Society of Mechanical Engineers, Vancouver, BC, Canada, 12–18 November 2010; pp. 1251–1258.
26. Velmurugan, V.; Srithar, K. Performance analysis of solar stills based on various factors affecting the productivity—A review. *Renew. Sustain. Energy Rev.* **2011**, *15*, 1294–1304. [CrossRef]
27. Sathyamurthy, R.; El-Agouz, E. Experimental analysis and exergy efficiency of a conventional solar still with Fresnel lens and energy storage material. *Heat Transf. Asian Res.* **2019**, *48*, 885–895. [CrossRef]
28. Abdelsalam, T.I.; Abdel-Mesih, B. An Experimental Study on the Effect of Using Fresnel Lenses on the Performance of Solar Stills. In Proceedings of theInternational Congress on Energy Efficiency and Energy Related Materials (ENEFM2013), Antalya, Turkey, 9–12 October 2013; pp. 353–362.
29. Sriram, V.; Kondraganti, V.; Lokireddy, C.T.R.; Jeevahan, J.; Joseph, G.B.; Raj, R.B.D.; Mageshwaran, G.; Venkatesh, K.; Reddy, L.C.T. Investigation of effect of the Fresnel lens on the performance of the double slope single basin solar still. *Int. J. Ambient. Energy* **2019**, 1–6. [CrossRef]
30. Sales, M.T.B.F. Solar powered desalination system using Fresnel lens. *IOP Conf. Ser.: Mater. Sci. Eng.* **2016**, *162*. [CrossRef]
31. Muraleedharan, M.; Singh, H.; Udayakumar, M.; Suresh, S. Modified active solar distillation system employing directly absorbing Therminol 55–Al_2O_3 nano heat transfer fluid and Fresnel lens concentrator. *Desalination* **2019**, *457*, 32–38. [CrossRef]
32. Fath, H.E.; Hosny, H. Thermal performance of a single-sloped basin still with an inherent built-in additional condenser. *Desalination* **2002**, *142*, 19–27. [CrossRef]
33. Abu-Arabi, M.; Zurigat, Y.; Al-Hinai, H.; Al-Hiddabi, S. Modeling and performance analysis of a solar desalination unit with double-glass cover cooling. *Desalination* **2002**, *143*, 173–182. [CrossRef]
34. Voropoulos, K.; Mathioulakis, E.; Belessiotis, V. Analytical simulation of energy behavior of solar stills and experimental validation. *Desalination* **2003**, *153*, 87–94. [CrossRef]
35. Singh, H.; Tiwari, G. Monthly performance of passive and active solar stills for different Indian climatic conditions. *Desalination* **2004**, *168*, 145–150. [CrossRef]

36. Janarthanan, B.; Chandrasekaran, J.; Kumar, S. Evaporative heat loss and heat transfer for open- and closed-cycle systems of a floating tilted wick solar still. *Desalination* **2005**, *180*, 291–305. [CrossRef]
37. Shukla, S.; Sorayan, V. Thermal modeling of solar stills: An experimental validation. *Renew. Energy* **2005**, *30*, 683–699. [CrossRef]
38. Tiwari, A.K.; Tiwari, G. Effect of water depths on heat and mass transfer in a passive solar still: In summer climatic condition. *Desalination* **2006**, *195*, 78–94. [CrossRef]
39. Khalifa, A.J.N.; Hamood, A.M. Performance correlations for basin type solar stills. *Desalination* **2009**, *249*, 24–28. [CrossRef]
40. Tanaka, H.; Nakatake, Y. Increase in distillate productivity by inclining the flat plate external reflector of a tilted-wick solar still in winter. *Sol. Energy* **2009**, *83*, 785–789. [CrossRef]
41. Madhlopa, A.; Johnstone, C. Numerical study of a passive solar still with separate condenser. *Renew. Energy* **2009**, *34*, 1668–1677. [CrossRef]
42. Dev, R.; Tiwari, G. Characteristic equation of a hybrid (PV-T) active solar still. *Desalination* **2010**, *254*, 126–137. [CrossRef]
43. Kumar, S.; Tiwari, G.; Gaur, M. Development of empirical relation to evaluate the heat transfer coefficients and fractional energy in basin type hybrid (PV/T) active solar still. *Desalination* **2010**, *250*, 214–221. [CrossRef]
44. Ahsan, A.; Imteaz, M.; Dev, R.; Arafat, H.A. Numerical models of solar distillation device: Present and previous. *Desalination* **2013**, *311*, 173–181. [CrossRef]
45. Murugavela, K.K.; Anburaja, P.; Hansonb, R.S.; Elangoc, T. Progresses in inclined type solar stills. *Renew. Sustain. Energy Rev.* **2013**, *20*, 304–377.
46. Ebaid, M.S.Y.; Ammari, H. Modeling and analysis of unsteady-state thermal performance of a single-slope tilted solar still. *Renew. Wind. Water Sol.* **2015**, *2*, 128. [CrossRef]
47. Hidouri, K.; Benhmidene, A.; Chaouachi, B.; Ravishankar, S. Comparative Study for Evaluation of Mass Flow Rate for Simple Solar Still and Active with Heat Pump. *J. Water Environ. Nanotechnol.* **2017**, *2*, 157–165.
48. Mu, L.; Xu, X.; Williams, T.; Debroux, C.; Gomez, R.C.; Park, Y.H.; Wang, H.; Kota, K.; Xu, P.; Kuravi, S. Enhancing the performance of a single-basin single-slope solar still by using Fresnel lens: Experimental study. *J. Clean. Prod.* **2019**, *239*, 118094. [CrossRef]
49. El-Sebaii, A.A.; Al-Ghamdi, A.A.; Al-Hazmi, F.S.; Faidah, A.S. Thermal performance of a single basin solar still with PCM as a storage medium. *Appl. Energy* **2009**, *86*, 1187–1195. [CrossRef]
50. Nafey, A.S.; Abdelkader, M.; Abdelmotalip, A.; Mabrouk, A.A. Enhancement of solar still productivity using floating perforated black plate. *Energy Convers. Manage.* **2002**, *43*, 937–946. [CrossRef]
51. Tiwari, G. Madhuri Effect of water depth on daily yield of the still. *Desalination* **1987**, *61*, 67–75. [CrossRef]
52. Agrawal, A.; Rana, R.; Srivastava, P.K. Heat transfer coefficients and productivity of a single slope single basin solar still in Indian climatic condition: Experimental and theoretical comparison. *Resour. Technol.* **2017**, *3*, 466–482. [CrossRef]
53. Dunkle, R.V. Solar water distillation: The roof type still and a multiple effect diffusion still. In Proceedings of the International Heat Transfer Conference, Boulder, CO, USA, 28 August–1 September 1961; p. 895.
54. Sharshir, S.; Elsheikh, A.; Peng, G.; Yang, N.; El-Samadony, M.; Kabeel, A. Thermal performance and exergy analysis of solar stills—A review. *Renew. Sustain. Energy Rev.* **2017**, *73*, 521–544. [CrossRef]
55. Tiwari, G.N.; Garg, P.H. Effect of water flow over the glass cover of a single basin solar still with an intermittent flow of waste hot water in the basin. *Energy Convers. Manag.* **1985**, *25*, 315–322. [CrossRef]
56. Singh, A.; Tiwari, G. Thermal evaluation of regenerative active solar distillation under thermosyphon mode. *Energy Convers. Manag.* **1993**, *34*, 697–706. [CrossRef]
57. Kavathekar, A.; Prakash, J. Performance prediction of a regenerative solar still. *Sol. Wind. Technol.* **1986**, *3*, 119–125.
58. El-Samadony, Y.; El-Maghlany, W.M.; Kabeel, A. Influence of glass cover inclination angle on radiation heat transfer rate within stepped solar still. *Desalination* **2016**, *384*, 68–77. [CrossRef]
59. Edalatpour, M.; Kianifar, A.; Ghiami, S. Effect of blade installation on heat transfer and fluid flow within a single slope solar still. *Int. Commun. Heat Mass Transf.* **2015**, *66*, 63–70. [CrossRef]
60. Chen, Z.; Yao, Y.; Zheng, Z.; Zheng, H.; Yang, Y.; Hou, L.; Chen, G. Analysis of the characteristics of heat and mass transfer of a three-effect tubular solar still and experimental research. *Desalination* **2013**, *330*, 42–48. [CrossRef]

61. Gupta, B.; Mandraha, T.K.; Edla, P.J.; Pandya, M. Thermal modeling and efficiency of solar water distillation: A review. *Am. J. Eng. Res.* **2013**, *2*, 203–213.
62. Velmurugan, V.; Kumaran, S.; Prabhu, N.; Srithar, K. Productivity enhancement of stepped solar still: Performance analysis. *Therm. Sci.* **2008**, *12*, 153–163. [CrossRef]
63. Velmurugan, V.; Kumar, K.N.; Haq, T.N.; Srithar, K. Performance analysis in stepped solar still for effluent desalination. *Energy* **2009**, *34*, 1179–1186. [CrossRef]
64. Dev, R.; Tiwari, G. Characteristic equation of a passive solar still. *Desalination* **2009**, *245*, 246–265. [CrossRef]
65. Zurigat, Y.H.; Abu-Arabi, M.K. Modelling and performance analysis of a regenerative solar desalination unit. *Appl. Therm. Eng.* **2004**, *24*, 1061–1072. [CrossRef]
66. Velmurugan, V.; Deenadayalan, C.; Vinod, H.; Srithar, K. Desalination of effluent using fin type solar still. *Energy* **2008**, *33*, 1719–1727. [CrossRef]
67. Rubio, E.; Fernández, J.L.; Porta-Gándara, M.A.; Rubio-Royo, E. Modeling thermal asymmetries in double slope solar stills. *Renew. Energy* **2004**, *29*, 895–906. [CrossRef]
68. Tiwari, G.; Shukla, S.; Singh, I. Computer modeling of passive/active solar stills by using inner glass temperature. *Desalination* **2003**, *154*, 171–185. [CrossRef]
69. Macdonald, G.M. Water, climate change, and sustainability in the southwest. *Proc. Natl. Acad. Sci.* **2010**, *107*, 21256–21262. [CrossRef] [PubMed]
70. Pakdel, M.A.; Hedayatizadeh, M.; Tabatabaei, S.M.; Niknia, N. An experimental study of a single-slope solar still with innovative side-troughs under natural circulation mode. *Desalination* **2017**, *422*, 174–181. [CrossRef]
71. Haddad, Z.; Chaker, A.; Rahmani, A. Improving the basin type solar still performances using a vertical rotating wick. *Desalination* **2017**, *418*, 71–78. [CrossRef]